

# BATCLIP: Bimodal Online Test-Time Adaptation for CLIP

Sarthak Kumar Maharana<sup>1</sup>, Baoming Zhang<sup>1</sup>, Leonid Karlinsky<sup>2</sup>, Rogerio Feris<sup>2</sup>, Yunhui Guo<sup>1</sup>

<sup>1</sup>The University of Texas at Dallas <sup>2</sup>MIT-IBM Watson AI Lab  
{sarthak.maharana, yunhui.guo}@utdallas.edu

## Abstract

*Although open-vocabulary classification models like Contrastive Language Image Pretraining (CLIP) have demonstrated strong zero-shot learning capabilities, their robustness to common image corruptions remains poorly understood. Through extensive experiments, we show that zero-shot CLIP lacks robustness to common image corruptions during test-time, necessitating the adaptation of CLIP to unlabeled corrupted images using test-time adaptation (TTA). However, we found that existing TTA methods have severe limitations in adapting CLIP due to their unimodal nature. To address these limitations, we propose BATCLIP, a bimodal **online** TTA method designed to improve CLIP’s robustness to common image corruptions. The key insight of our approach is not only to adapt the visual encoders for improving image features but also to strengthen the alignment between image and text features by promoting a stronger association between the image class prototype, computed using pseudo-labels, and the corresponding text feature. We evaluate our approach on benchmark image corruption datasets and achieve state-of-the-art results in online TTA for CLIP. Furthermore, we evaluate our proposed TTA approach on various domain generalization datasets to demonstrate its generalization capabilities.*

## 1. Introduction

The emergence of large pre-trained vision-language models (VLMs), such as CLIP [38], has led to their widespread adoption in various visual recognition tasks, including segmentation [24, 29], detection [2, 27], classification [60, 61], and image generation [39, 40, 52]. Thanks to supervision from massive corpora of paired language and image data, VLMs like CLIP demonstrate strong zero-shot capabilities for these downstream tasks.

Despite CLIP’s successes in such important applications, its robustness when faced with corrupted images remains largely underexplored. Our motivation stems from the fact that the vision perception system of humans exhibits a level of robustness that real-world vision systems are yet to

achieve. For example, models deployed for safety-critical applications like autonomous driving [1], could face rapid distributional shifts of blurriness, pixel changes, snowy nights, or other weather conditions [42]. In particular, our findings on the zero-shot performance of CLIP with a ResNet-101 [17] vision backbone reveals that the accuracy on the test set of CIFAR100 [22] with *Gaussian* noise of severity level 5, plummets to 10.79% from 49% on the clean set. Similar trends are observed with ViT-B/16, -B/32, and -L/14 [11] as backbones. The performance degradation caused by image corruption can have significant consequences in real-world scenarios, particularly in safety-critical applications like self-driving cars.

One effective approach to improving model performance under distribution shift is test-time adaptation (TTA) [9, 53], where a pre-trained model is directly adapted to unlabeled test batches, without access to the source dataset. Moreover, given the abundance of unlabeled data available in the wild, there is a growing need for *online* adaptation to streaming data, with a *single* forward pass, ensuring privacy, real-time performance [31], and preventing *catastrophic forgetting* [13] of source knowledge. Several online TTA methods proposed in the literature have been effective in mitigating domain shifts [4, 35, 41, 43, 48, 53]. In this paper, we use the terms distributions and domains interchangeably.

While there have been few works on using CLIP for **online** TTA [10, 21, 45], they come with certain limitations. For example, test-time prompt tuning (TPT) [45] tunes the text prompts on the text encoder alone and generates multiple random augmented views, for each test image. The text prompts, initialized to pre-trained values, are optimized by minimizing the marginal entropy of the confident model predictions. The prompts are reset after adaptation to each image. However, such a method is expensive and slow due to performing multiple forward passes through the vision encoder of CLIP, for each image. Also, it relies on hand-crafted prompts for initialization, making it impractical at test-time. Another recent approach, Vision-Text-Space Ensemble (VTE) [10], uses an ensemble of different prompts as input to CLIP’s text encoder while keeping both the encoders frozen. Since the vision encoder is frozen, it strug-

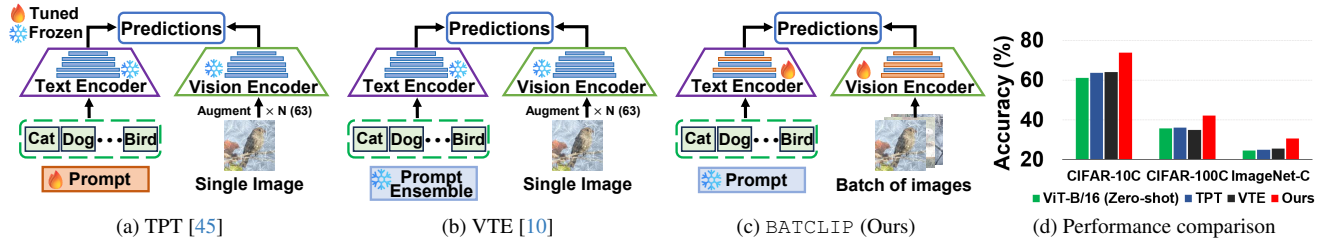


Figure 1. Comparison of BATCLIP with other **online** TTA approaches using CLIP. a) TPT [45] optimizes text prompts only for a single test image, making it *unimodal*. b) VTE [10] considers an ensemble of prompts without model updates. Both methods consider the generation of multiple augmentations of the test image. c) BATCLIP is a *bimodal* approach, that adapts the LayerNorm parameters of the vision and text encoders, maximizing alignment between class prototypes and text features while increasing the inter-class separability of prototypes.

gles to effectively adapt to images with severe noise.

While TPT effectively improves CLIP’s test generalization by dynamically tuning the text prompts, it remains primarily a *unimodal* approach. This limits the capacity of a multimodal model like CLIP to fully leverage its multimodal nature for adaptation. Specifically, it prevents the encoders from jointly adjusting their features, resulting in suboptimal alignment between the visual and text modalities after adaptation. For instance, when a test image includes common corruptions, the text prompts adapt, but the vision encoder features remain fixed. As a result, the learned prompts lack awareness of the test image distribution, leading to a less effective adaptation.

To address these core limitations, we propose, BATCLIP, a *bimodal* adaptation approach of CLIP for **online** TTA specifically, where both the visual and text encoders are jointly adapted by exploiting CLIP’s shared feature space of images and text. The overall objective is to achieve a strong alignment between image features and text features to enable more effective multimodal learning and adaptation. The adaptation procedure is two-fold: 1) Inspired by [54, 58] for efficient fine-tuning, we only adapt the norm layers, i.e., *LayerNorm* parameters of both encoders. However, such a model update does not consider the alignment of the encoder features. Therefore, to improve the alignment between class-specific visual and text features, we introduce a projection matching loss that maximizes the projection of the visual class prototypes with their corresponding text features. 2) To learn more discriminative visual features, we enhance the cosine distance between class prototypes, computed using pseudo-labels, to promote a more distinct separation in the image feature space. Our method is general-purpose, with no reliance on multiple prompt templates [15, 34, 36] or their ensembles, unlike VTE. We leverage batches of test samples for TTA, rather than focusing on single-image test adaptation, which makes our method fast. In the Supplementary, we show several examples of classification results, as a comparison. Figure 1d shows that with a *bimodal online* test-time adaptation (TTA) setup for CLIP, the proposed approach achieves a significant improvement compared to TPT and

VTE.

Our main contributions are as follows:

- We start with an in-depth analysis of CLIP’s zero-shot performance across different visual backbones on an established benchmark on common image corruptions [18], at test-time, for varying severity levels. We found that while CLIP shows strong performance on clean images, its performance drops notably on corrupted images.
- To address the *unimodal* limitations highlighted earlier, we propose BATCLIP, a *bimodal online* test-time adaptation method for CLIP encoders, designed to enhance alignment by maximizing the projection of class-wise prototypes onto their corresponding text features. Simultaneously, we increase the cosine distance between class prototypes to encourage learning of more discriminative features, making the test adaptation process more flexible and robust.
- We conduct extensive experiments benchmarking the proposed method against established TTA baselines and others using CLIP on CIFAR-10C, CIFAR-100C, and ImageNet-C [18]. To generalize our method beyond common corruptions, we evaluate on various domain generalization datasets [14]-OfficeHome [51], PACS [25], VLCS [12], and Terra Incognita [3]. Overall, our approach achieves state-of-the-art performance for CLIP adaptation at test-time on various domain shifts.

## 2. Related Works

**Online Test-Time Adaptation (TTA).** The objective of online TTA is to adapt a pre-trained model, with no access to the source data, to incoming batches of unlabelled test data of a specific domain [4, 6, 35, 41, 43, 48, 53, 57]. In this approach, the model is reset to its pre-trained state after adapting to each target domain. As the updates are performed online, TENT [53] updates the affine parameters of the normalization layers and minimizes the entropy [44] of the model predictions. RoTTA [54] proposes a robust feature normalization method, leveraging a memory bank to track test data distribution and a teacher-student framework for adaptive reweighting and updates. RPL [41] argues that self-learning during adaptation via entropy minimiza-

tion and pseudo-labels is beneficial. They propose the usage of a generalized cross-entropy loss for adaptation. SAR [35] filters noisy test samples that cause a performance drop identified from the gradient space. However, none of these works utilize CLIP for TTA.

**TTA using CLIP.** Lately, VLMs like CLIP have found extensive applications for *online* TTA [10, 21, 30, 45, 59]. TPT [45] was the first work to propose prompt tuning using CLIP at test-time in an online manner. However, this method is computationally intensive for generating multiple views, per image. A similar line of work was done in VTE [10] where ensembles are created in the text and vision space without any CLIP parameter update. Ma et al. [30] explore the idea of self-supervised contrastive learning for prompt learning. Another brewing line of TTA work focuses on realistic TTA. StatA [55] proposes a regularization anchor term, for zero-shot CLIP, handling variable number of effective classes within a test batch, often overlooked in existing TTA methods [20, 32, 56] on other visual benchmarks [61].

Another set of TTA works using CLIP [15, 34, 36] leverage information from multiple prompt templates. WATT [36] adapts CLIP’s vision encoder, weight-averaging the adapted weights from multiple prompt templates, for each test batch, over several optimization steps. Similarly, CLIPArTT [15] enhances text supervision from the support of pseudo-labels. Mishra et al. [34] pose pseudo-labeling as an Optimal Transport [7] problem by distilling knowledge from multiple text prototypes, for several iterations. Please note that the TTA setups here largely differ from our **online** TTA setup [53].

While promising, these approaches have key limitations. Firstly, multiple gradient descent steps on a test batch can result in large parameter shifts, leading to the loss of CLIP’s source knowledge i.e., *catastrophic forgetting* [13]. No regularization strategies have been proposed to restrict the loss of CLIP’s pretrained knowledge. Secondly, these methods are not favorable for real-time deployment where fast and on-the-fly test-adaptation must meet privacy and memory constraints. Thirdly, relying on multiple prompt templates, at test-time, is impractical. We discuss this in Section 3.

### 3. Zero-shot performance analysis of CLIP to common image corruptions

While CLIP generalizes well to new concepts across vision-language modalities [5, 16], its performance under image corruptions is less explored. This section evaluates CLIP’s zero-shot capabilities in real-world scenarios with domain shifts caused by common corruptions, focusing on two primary areas: *zero-shot performance and the need for adaptation to address domain shifts effectively*.

**Vision Backbones.** We evaluate the robustness with a ResNet-101 (RN101) vision backbone [17] and three ViT

backbones (ViT-B/16, ViT-B/32, and ViT-L/14) [11]. The models are tested on their zero-shot classification performance.

**Datasets.** For all the experiments in this paper, we utilize the CIFAR-10C, CIFAR-100C, and ImageNet-C [18] datasets, which are standard benchmark datasets to evaluate the robustness of vision models [18]. Each dataset contains 15 distinct corruption types as tasks (e.g., Gaussian noise, Shot noise, ...). Each corruption is applied at 5 different severity levels to the test sets of CIFAR10, CIFAR100 [22], and ImageNet [8], acting as source test sets, and allowing us to systematically evaluate the model’s performance under increasing degrees of image degradation.

**Online TTA Problem Setup.** Each corruption type of a certain severity level, posed as a task  $\mathcal{T}_i$  with  $\mathcal{B}$  test batches, is sequentially presented to CLIP’s vision encoder for model predictions, with each test batch being revealed one at a time for a *single* forward pass. Let a batch of images from task  $\mathcal{T}_i$ , at time step  $t$ , be denoted as  $x_i^t$ . For the prompt template, unless explicitly mentioned, we always use the generic “a photo of a <CLS>.” to generate  $C$  text representations ( $\mathcal{Z} = \{z_c\}_{c=1}^C$ ), where  $C$  is the total number of classes. Let  $f_{vis}$  and  $f_{txt}$  denote CLIP’s vision and text encoder, respectively. The visual feature of the  $k^{th}$  image in batch  $x_i^t$  is  $v_{k,i}^t = f_{vis}(x_{k,i}^t)$ . The likelihood of it belonging to class  $c$  is,

$$p(y = c | x_{k,i}^t) = \frac{\exp(\text{sim}(v_{k,i}^t, z_c) / \tau)}{\sum_j \exp(\text{sim}(v_{k,i}^t, z_j) / \tau)} \quad (1)$$

$$\text{sim}(v, z) = \frac{v^T \cdot z}{\|v\|_2 \cdot \|z\|_2}$$

where  $\text{sim}(\cdot)$  is the cosine similarity and  $\tau$  is the softmax temperature from CLIP’s pre-training stage. The text features  $\mathcal{Z}$ , in zero-shot evaluation, are always pre-computed. We also draw a comparison with CLIP performance on respective source test sets and follow this implementation<sup>1</sup>. Throughout this paper, the same TTA problem setup is used, unless mentioned otherwise. This TTA setup differs from the TTA setups of [15, 34, 36].

#### 3.1. Sensitivity of CLIP to image corruption severity

We analyze CLIP’s zero-shot performance by progressively increasing corruption severity for RN101 and ViT-B/16 vision backbones. We illustrate mean accuracy and overall performance in Figure 2. Despite CLIP’s robust multimodal feature space, accuracy drops significantly with an increase in corruption severity, regardless of the backbone. Specifically, for CIFAR-10C with a ViT-B/16 backbone, we observe accuracy as low as 37.92%, at a severity level of 5, for *Gaussian* noise. Similarly, for CIFAR-100C and ImageNet-C, the mean accuracy rates are as low as 35.79%

<sup>1</sup>[https://github.com/LAION-AI/CLIP\\_benchmark](https://github.com/LAION-AI/CLIP_benchmark)

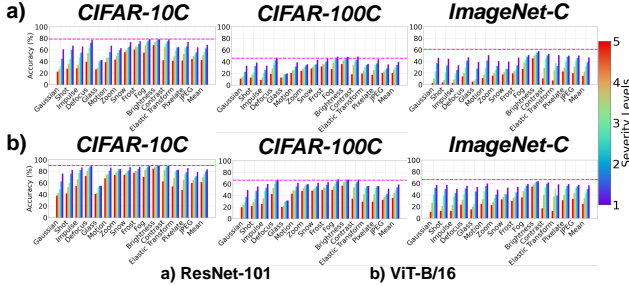


Figure 2. Task-wise mean accuracy (%) of zero-shot CLIP across corruption severity levels. [Top]: ResNet-101 backbone. [Bottom]: ViT-B/16 backbone. **Dashed lines** show zero-shot CLIP performance on corresponding source test sets (clean).

and 24.51% at a severity level of 5, respectively. Results on additional vision backbones are in the Supplementary.

**Analysis.** CLIP’s zero-shot classification accuracy varies across models and datasets. Comparing the results to source test sets, for CIFAR10, RN101 achieves 78.8%, improving to 90.1% with ViT-B/16. On CIFAR100, accuracies are 46.1% and 66.6%, respectively. For ImageNet, RN101 scores 61.2%, while ViT-B/16 reaches 67.7%. More importantly, the key takeaway from Figure 2 is — even a slight increase in severity to level 1, for a majority of the corruption tasks, leads to a noticeable drop in accuracy. One plausible explanation for CLIP’s subpar performance is that the parameters of  $f_{vis}$  were not optimized for such corruptions during pre-training. In zero-shot classification, the visual features from a given domain may lack the robustness and richness necessary to align well with their corresponding text features. This results in lower likelihoods and thus, higher misclassification rates.

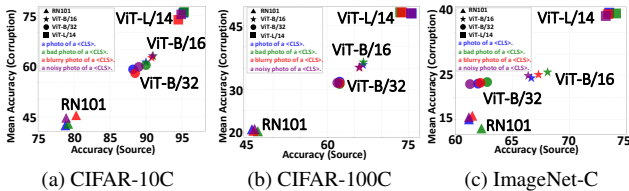


Figure 3. Mean classification accuracy (in %) across all the corruption types vs. accuracy on corresponding source test sets, evaluated using various prompt templates and across vision backbones.

### 3.2. Sensitivity of CLIP to prompt templates

In this analysis, we evaluate the impact of prompt engineering by providing “relevant” prompt templates to  $f_{txt}$  for TTA. Each prompt adds context to help CLIP extract more relevant text features. We report the mean classification accuracy (in %) across RN101, ViT-B/16, ViT-B/32, and ViT-L/14 backbones at an image corruption severity level of 5 for all datasets, with results presented in Figure 3. For each dataset, the x-axis is the source accuracy and y-axis is the mean accuracy, across 15 tasks.

**Analysis.** It is interesting to observe that, irrespective of the

backbones used, we do not see any drastic changes in the mean accuracy, for different “relevant” prompt templates. However, the major concern arises in the performance gap of each model and the zero-shot CLIP performance on the corresponding source test set, for the same prompt template. This discrepancy highlights the limited robustness of CLIP’s text encoder  $f_{txt}$  to prompt selection in the context of image corruption. A key reason for this is that, *despite the use of “relevant” prompts, the text and visual features remain largely independent and unaware of one another.*

As expected, RN101 performs worse than the ViT-based backbones, primarily due to its lack of global attention-based modeling inherent to transformers [50]. Therefore, for the remainder of the experiments in this paper, we focus on ViT-based backbones, specifically ViT-B/16.

### Unsuitability of prompt template selection at test-time.

Additionally, at test-time, it is impractical to perform prompt engineering or optimize prompt vectors since 1) Choosing different prompt templates for generating text features is extremely tedious and time-consuming. As discussed in Section 2, CLIP TTA works [15, 34, 36] use various prompt templates, making it unrealistic. 2) In real-time deployment involving prompt-tuning, such prompts cannot quickly estimate the distribution of incoming test batches. TPT [45] optimizes pre-trained text prompts for each test image, turning out to be suboptimal since the prompts are optimized ignorant of the distribution of the test image.

## 4. Proposed Methodology

The comprehensive analysis in Section 3 reveals that the zero-shot vision encoder  $f_{vis}$  of CLIP is very sensitive to image corruption with increasing severity. Similarly, the performance of the text encoder  $f_{txt}$  is invariant to the different text prompt templates and is also impractical to tune at test-time. Therefore, for effective adaptation, both the image and text encoders of CLIP need to be *adapted* to the incoming domain of test batches. We illustrate our proposed framework, BATCLIP, in Figure 4.

### From unimodal adaptation to bimodal adaptation.

The goal of TTA is to enhance a model’s performance in the current domain to ensure accurate predictions. To handle the complexities of CLIP adaptation to a specific domain of image corruption, we dissect our analysis of each encoder’s adaptation. Consider the *unimodal* adaptation of the vision encoder  $f_{vis}$  via entropy minimization [53]. While the image features are adjusted for a specific test batch and domain, the text features remain fixed, still being optimized for the data from CLIP pre-training, as seen in Figure 4 (top row). Likewise, if only the text encoder  $f_{txt}$  is updated in this manner, the generated text features may not align properly with the distribution of the incoming data, potentially causing misalignment between the image and text features, missing in the ideas of TPT [45] and VTE [10].

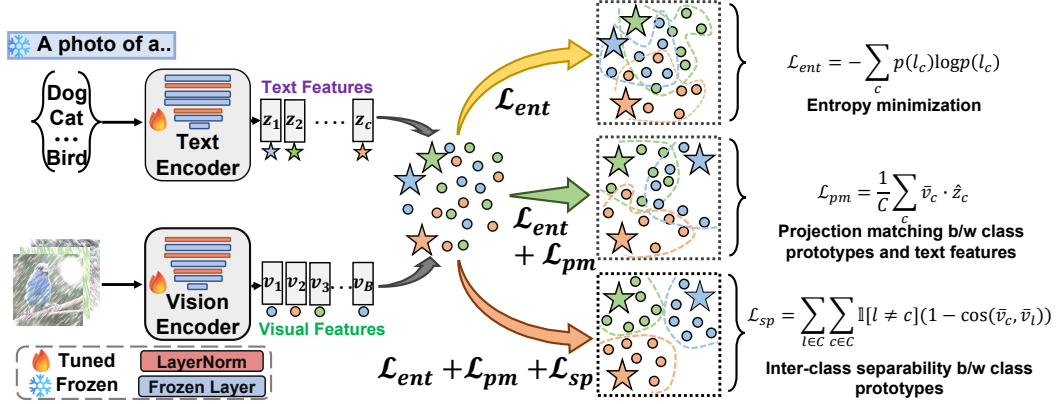


Figure 4. Illustration of our proposed approach: BATCLIP not only adapts the visual encoder for highly discriminative image features but also promotes a strong alignment between image and text features by adapting the text encoder too, leading to improved performance following test-time adaptation. We adapt only the LayerNorm parameters of CLIP encoders.

To benefit from the feature space and learn richer representations across both modalities, we propose adapting both  $f_{vis}$  and  $f_{txt}$  to a domain, enabling an input-aware knowledge transfer between the encoders and enhancing domain-specific adaptation. While the encoders can be updated based on entropy minimization, they come with inherent limitations. Though entropy models the prediction uncertainty, it does not guarantee increasing the likelihood of alignment between the image and text features. Additionally, due to the image corruption, for images within a test batch, there could be a possible overlap of visual features belonging to different classes [23]. The robustness of CLIP would be challenged in such a case. To address these limitations, we propose two loss components that facilitate a more effective *bimodal* adaptation of CLIP to new domains at test-time. The losses focus on maximizing separation between the visual and text features while increasing decision boundaries.

**Projection matching between the visual and text features.** We propose learning visual and text features that are domain-specific and mutually aware by *jointly updating the encoders*, as in Figure 4 (middle row), opposed to a *unimodal*. From Eq. 1, the visual feature  $v_{k,i}^t$  of the  $k^{th}$  image in batch  $x_i^t$  needs to have a high similarity with the text feature  $z_c$  of class  $c$  for good alignment. To quantify this similarity, an approach is to project the visual feature onto the text feature *i.e.*, compute the scalar projection —  $v_{k,i}^t \cdot \hat{z}_c$ , where  $\hat{z}_c$  is the normalized text feature of  $z_c$  *i.e.*,  $\hat{z}_c = \frac{z_c}{\|z_c\|_2}$ . Geometrically speaking, maximizing this projection leads to more similarity between the corresponding features and hence, a better alignment. However, computing such a projection could have limitations. Within the test batch, due to the image corruption, the pseudo-labels could be wrong/noisy. Instead, we propose modeling the projection of the class prototype with its corresponding text

feature. A prototype is useful, in such a scenario, because it encompasses the entire class distribution without relying on individual visual features [46]. In particular, we compute a class prototype as,

$$\bar{v}_c = \frac{1}{\sum_{k=1}^{\mathcal{B}} \mathbb{1}[\hat{y} = c]} \sum_{k=1}^{\mathcal{B}} \mathbb{1}[\hat{y} = c] v_{k,i}^t \quad (2)$$

$$\hat{y} = \operatorname{argmax}_c p(y|x_i^t)$$

*i.e.*, for the current test batch, we compute the mean feature of all the support visual features constituting a class  $c$ , based on the computed pseudo-labels (Eqs. 1 and 2), where  $\hat{y}$  refers to the pseudo-labels computed via Eq. 1 and  $\bar{v}_c$  is the class prototype of class  $c$ . Based on the class prototype, the projection matching loss is,

$$\mathcal{L}_{pm} = \frac{1}{C} \sum_c \bar{v}_c \cdot \hat{z}_c \quad (3)$$

Eq. 3 encourages a class prototype to have a larger projection on its corresponding text feature. In this way, during the adaptation of CLIP to a certain domain, both encoders learn to generate richer visual and text features with maximum alignment by maximizing Eq. 3. Figure 4 (middle row) shows such an illustration.

**Inter-class separability between class prototypes.** The projection matching loss introduced in Eq. 3 encourages the  $f_{vis}$  and  $f_{txt}$  encoders to produce domain-specific, well-aligned, and input-aware features via jointly updating the encoders. However, when TTA occurs at a batch level with image corruption, visual features within the batch could overlap, leading CLIP to poorly differentiate between classes. This ultimately hinders effective class separation. Hence, with a desire to obtain separation between visual features from different classes, as illustrated in Figure 4 (last row), we propose maximizing the distance between the

class prototypes. Since the visual and text features align across modalities via Eq. 3, class separation, in addition, is needed for good generalization, robustness, and adaptation. Therefore, we additionally incorporate a loss to increase the cosine distance between the class prototypes,

$$\mathcal{L}_{sp} = \sum_{l \in C} \sum_{c \in C} \mathbb{1}[l \neq c] (1 - \cos(\bar{v}_c, \bar{v}_l)) \quad (4)$$

**Optimization.** TENT [53] optimizes the output logits by minimizing the entropy [44]. When applied to CLIP, the entropy, with output logits  $l$ , is defined as,

$$\mathcal{L}_{ent} = - \sum_c p(l_c) \log p(l_c) \quad (5)$$

where  $p(l_c)$  is the likelihood for class  $c$  that is computed via Eq. 1. The overall optimization objective for our approach is as,

$$\operatorname{argmin}_{\phi_v, \phi_t} (\mathcal{L}_{ent} - \mathcal{L}_{pm} - \mathcal{L}_{sp}) \quad (6)$$

where  $\phi_v$  and  $\phi_t$  refer to the LayerNorm parameters of  $f_{vis}$  and  $f_{txt}$ , respectively.

**Motivation of choice of parameters.** Through thorough experimentation, Zhao et al. [58] demonstrate that fine-tuning *LayerNorm* (LN) parameters in attention-based models leads to yielding strong results on multimodal tasks. This also brings a reduction in trainable parameters. Updating normalization layers has also been deeply studied in tasks involving domain shifts [26]. Motivated by these works, we update the *LayerNorm* parameters of both CLIP encoders. This constitutes updating  $\sim 0.044\%$  of all parameters. For every new task/corruption, we reset the model parameters following TENT [53] i.e., we perform a single domain TTA. In summary, our *bimodal online* test-time adaptation approach jointly updates the LayerNorm parameters of the CLIP encoders that are optimized synergistically through loss components aware of the input domain, leading to a more robust multimodal learning process.

## 5. Experiments and Results

**Baselines.** We compare our approach with zero-shot CLIP (ZS), state-of-the-art online TTA methods adopted for CLIP following [10] i.e., TENT [53], RoTTA [54], RPL [41], and SAR [35]. We update only the vision encoder  $f_{vis}$  for such a setup. We benchmark against other online TTA methods using CLIP - TPT [45] and VTE [10]. Based on the discussion in Section 2, we adapt the two variants of WATT [36], for our setup, to WATT-P\* and WATT-S\*, while maintaining method consistency. For a “fairer” comparison, on each test batch, the model is adapted once using each of the suggested 8 prompt templates. Note that this setup is **not online** yet. In addition, CLIP parameters are reset after every task. We report the results on CIFAR-10C

and CIFAR-100C only, based on their suggested settings. On ImageNet-C, we also report results against online StatA [55], based on their chosen hyperparameters. The model predictions can then be computed as in Eq. 1. We mention the details of each TTA method in the Supplementary.

**Implementation Details.** We query the text encoder  $f_{txt}$  with a general prompt template “a photo of a <CLS>.” for all the datasets, as motivated earlier. We optimize both the vision encoder  $f_{vis}$  and text encoder  $f_{txt}$ . For CIFAR-10C, we use an AdamW optimizer at a learning rate of  $10^{-3}$ . Similarly, for CIFAR-100C and ImageNet-C, Adam and AdamW optimizers are respectively used, at a fixed learning rate of  $5 \times 10^{-4}$ , with the model being reset after each task. For fairness to all the baselines, the batch sizes are set to 200, 200, and 64 for the datasets, following various TTA benchmarks, at a corruption severity level of 5 for each task. For WATT-P\* and WATT-S\*, we use the same templates and learning rates as mentioned in [36]. For StatA, the class correlation in a batch is controlled by a Dirichlet distribution ( $\gamma$ ). We report results for  $\gamma = 0.1$  (low correlation) and -1 (sequential). All experiments are run on a single NVIDIA RTX A5000 GPU using ViT-B/16 as the visual backbone. Results on ViT-B/32 are reported in the Supplementary.

### 5.1. Results: Online Test-Time Adaptation

**Results on CIFAR-10C, CIFAR-100C, and ImageNet-C.** We present the **online** TTA results in Table 1. While most TTA methods outperform zero-shot CLIP on average, BATCLIP consistently exceeds the performance of these methods across all datasets. SAR shows significant performance improvements over others. Although it performs similarly to our method on CIFAR-100C and ImageNet-C, BATCLIP outperforms SAR on CIFAR-10C, achieving improvements of 6.48%. While all the prior approaches operate solely in the vision space, our approach leverages CLIP’s joint vision-language feature space, resulting in superior TTA performance. For TTA approaches using CLIP, BATCLIP surpasses TPT and VTE across all tasks and datasets. For our WATT-P\* and WATT-S\* implementation, adaptation happens once on each prompt template for a batch. Interestingly, despite CLIP being *trained* on the batch by averaging adapted weights from multiple templates before inference, the performance remains subpar. This indicates that WATT [36] is not well suited for online TTA. In StatA [55],  $\gamma$  controls the number of effective classes in a batch, for zero-shot VLM adaptation. On ImageNet-C, the large drop in performance for each task indicates the need for CLIP adaptation to severe image degradation and the importance of relevant text features. In Figure 5, we show t-SNE [49] plots of visual and text features, of a few tasks, and compare them against zero-shot ViT-B/16 for CIFAR-10C. It highlights how our approach

Method	Venue	Corruption															Mean	
		Gaussian	Shot	Impulse	Defocus	Glass	Motion	Zoom	Snow	Frost	Fog	Brightness	Contrast	Elastic	Pixelate	JPEG		
CIFAR-10C	ZS	ICLR'21	37.92	41.7	54.42	71.75	40.89	67.93	73.62	73.89	77.35	70.22	84.45	62.36	53.81	47.65	59.43	61.16
	TENT	ICLR'21	15.49	18.28	38.12	81.59	21.73	76.32	82.35	<b>84.62</b>	82.19	80.60	<b>91.83</b>	80.55	63.52	58.57	54.71	62.03
	RoTTA	CVPR'23	39.17	42.90	55.41	72.18	41.32	68.02	74.01	74.38	78.01	70.80	84.80	63.19	54.62	49.32	60.15	61.89
	RPL	arXiv	15.47	17.43	40.73	<b>81.76</b>	20.08	69.89	<b>82.93</b>	84.43	83.19	81.84	91.80	79.42	64.89	54.07	54.90	61.52
	SAR	ICML'22	47.98	53.60	60.56	74.30	47.56	73.15	76.43	77.91	79.88	75.66	86.79	71.62	58.34	62.03	64.71	67.37
	TPT	NeurIPS'22	37.74	42.24	60.57	72.88	44.80	69.69	75.37	75.96	78.84	72.12	85.68	62.04	58.90	55.14	62.64	63.64
	VTE	ECCV-W'24	42.42	46.26	64.23	71.10	45.58	68.50	73.66	76.75	78.27	71.02	85.28	57.24	59.54	60.59	61.85	64.15
	WATT-P*	NeurIPS'24	44.70	49.66	60.48	74.35	46.33	72.21	76.28	78.18	80.97	74.90	87.66	68.63	58.35	56.13	63.47	66.15
	WATT-S*	NeurIPS'24	57.22	61.86	<b>67.63</b>	78.61	53.07	77.85	80.14	81.84	83.46	80.38	89.67	78.45	65.76	<b>68.63</b>	<b>67.67</b>	72.81
	Ours		<b>61.13</b>	<b>64.09</b>	65.76	80.51	<b>54.96</b>	<b>80.65</b>	81.94	83.04	<b>84.19</b>	<b>80.84</b>	88.95	<b>82.15</b>	<b>69.16</b>	62.68	66.64	<b>73.85</b>
CIFAR-100C	ZS	ICLR'21	19.64	21.40	25.26	42.54	20.03	43.17	47.95	48.35	49.74	41.57	57.02	34.58	29.15	23.96	32.43	35.79
	TENT	ICLR'21	7.60	8.21	8.33	51.81	7.95	<b>52.45</b>	55.34	54.16	36.17	50.92	65.63	<b>54.51</b>	36.52	<b>43.99</b>	35.81	37.96
	RoTTA	CVPR'23	20.65	22.22	26.17	42.48	20.26	42.90	47.88	48.75	49.92	41.86	57.00	34.52	29.27	25.08	32.88	36.12
	RPL	arXiv	6.44	7.09	7.09	<b>52.16</b>	11.81	52.33	<b>55.50</b>	<b>54.20</b>	38.83	<b>51.99</b>	<b>66.07</b>	54.45	<b>36.86</b>	42.83	<b>39.45</b>	38.47
	SAR	ICML'22	<b>25.30</b>	27.19	32.78	47.12	23.42	47.16	51.70	51.94	<b>52.48</b>	48.77	61.54	44.50	32.26	33.67	38.06	41.19
	TPT	NeurIPS'22	17.95	19.51	27.13	43.53	20.08	42.65	48.63	49.11	49.48	42.14	57.35	33.26	31.13	27.59	32.75	36.15
	VTE	ECCV-W'24	17.96	18.72	28.17	40.38	19.60	39.50	45.33	48.24	46.87	40.73	55.31	30.04	32.47	30.35	31.45	35.01
	WATT-P*	NeurIPS'24	20.53	22.22	27.3	43.14	17.51	42.37	48.17	47.31	49.34	41.49	57.07	35.29	27.75	25.83	31.89	35.81
	WATT-S*	NeurIPS'24	21.20	23.11	28.23	44.16	18.45	43.44	49.14	48.16	50.05	42.35	57.82	36.43	28.36	26.85	32.93	36.71
	Ours		24.91	<b>27.73</b>	<b>33.66</b>	50.11	<b>26.27</b>	48.49	54.85	52.35	51.62	48.38	63.27	45.21	34.74	32.38	37.31	<b>42.09</b>
ImageNet-C	ZS	ICLR'21	11.18	12.54	12.04	23.36	15.18	24.50	22.58	32.32	29.88	35.88	54.18	17.20	12.72	30.96	33.26	24.51
	TENT	ICLR'21	5.14	5.70	7.44	25.22	19.34	26.80	24.16	33.56	30.42	37.74	54.24	22.50	13.90	35.02	36.08	25.15
	RoTTA	CVPR'23	11.34	12.96	12.32	23.38	15.50	24.66	22.90	32.56	30.02	35.98	54.32	17.20	12.80	31.06	33.46	24.78
	RPL	arXiv	9.04	10.04	10.96	24.40	17.40	26.28	23.76	32.70	30.62	36.64	54.04	19.38	13.24	33.14	34.60	25.08
	SAR	ICML'22	17.96	20.46	20.68	25.72	23.04	29.52	26.04	34.92	32.74	39.00	55.00	27.14	19.64	36.66	37.50	29.73
	TPT	NeurIPS'22	8.48	9.46	10.20	23.98	15.16	25.10	24.00	33.94	32.12	37.08	55.64	16.54	13.68	34.06	33.58	24.87
	VTE	ECCV-W'24	9.18	10.76	10.78	24.72	14.30	24.36	25.24	35.38	32.46	38.16	55.56	16.14	14.26	38.72	33.98	25.60
	StatA ( $\gamma=0.1$ )	CVPR'25	10.56	11.22	10.86	22.11	14.12	22.39	20.85	31.39	29.90	34.63	53.32	16.00	12.46	29.55	32.79	23.47
	StatA ( $\gamma=-1$ )	CVPR'25	11.83	13.02	12.41	23.71	15.02	23.64	21.79	31.80	30.22	36.52	54.15	17.56	13.00	32.01	33.37	24.67
	Ours		<b>19.32</b>	<b>21.38</b>	<b>19.60</b>	<b>26.58</b>	<b>21.94</b>	<b>30.88</b>	<b>29.02</b>	<b>36.48</b>	32.00	<b>40.98</b>	<b>56.72</b>	<b>26.14</b>	<b>23.74</b>	37.67	<b>38.34</b>	<b>30.72</b>

Table 1. Mean accuracy (%) on CIFAR-10C, CIFAR-100C, and ImageNet-C - TTA mean accuracy of the 15 corruptions (tasks) at a severity level of 5, using ViT-B/16.

enhances alignment with text features, fosters better class separation, and forms more distinct clusters, leading to significant improvements. The Supplementary shows detailed t-SNE plots for CIFAR-10C and CIFAR-100C.

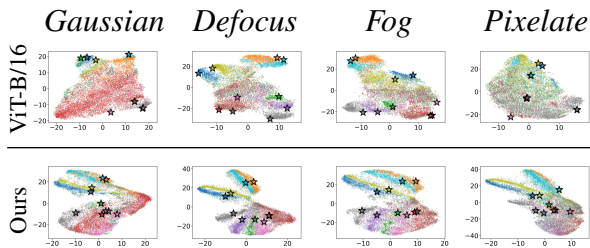


Figure 5. *BATCLIP* yields more discriminative visual features that exhibit stronger alignment with their corresponding text features. The t-SNE [49] plots show visual (○) and text (★) features for CIFAR-10C, comparing zero-shot ViT-B/16 with our approach.

## 5.2. Results: Domain Generalization Datasets

In this section, we evaluate our *BATCLIP* on commonly used domain generalization datasets [14] and benchmark against zero-shot ViT-B/16 (ZS), TENT, WATT-P\* and WATT-S\*. From Table 2, we observe that *BATCLIP* does better or comparable, across all datasets and domain shifts, to all the baselines. TENT matches zero-shot CLIP since

Dataset	Domain	ZS	TENT	WATT-P*	WATT-S*	Ours
OfficeHome	Art	78.29	79.4	80.35	<b>80.43</b>	79.86
	Clipart	64.03	63.18	66.85	<b>66.9</b>	66.44
	Product	87.11	88.42	87.5	87.54	<b>88.51</b>
	Real World	88.96	89.6	<b>90.04</b>	89.99	89.67
PACS	Art	97.22	<b>98.05</b>	97.75	97.75	97.56
	Cartoon	97.4	<b>97.65</b>	97.53	97.53	97.48
	Photo	99.58	99.58	99.59	99.52	<b>99.72</b>
	Sketch	86.23	<b>88.75</b>	88.52	88.65	87.76
VLCS	Caltech101	99.43	99.43	99.36	99.36	<b>99.51</b>
	LabelMe	68.15	68.14	66.92	68.49	<b>68.94</b>
	SUN09	73.4	73.4	74.53	74.68	<b>75.23</b>
	VOC2007	84.75	84.75	84.0	84.03	<b>85.6</b>
TerraInc	L38	20.3	20.3	27.79	29.08	<b>37.33</b>
	L43	31.52	31.52	33.98	<b>34.13</b>	32.71
	L46	28.98	28.98	27.07	28.13	<b>31.05</b>
	L100	52.35	52.35	43.59	42.32	<b>55.22</b>

Table 2. Accuracy on domain generalization datasets [14] with other domain shifts using a ViT-B/16 visual backbone.

LN normalization works per image across the features, independent of the batch statistics. We demonstrate that *BATCLIP* can be generalized and be robust to other various domain shifts, with a single step adaptation and global prompt template as opposed to WATT-P\* and WATT-S\* that use multiple prompt templates. The largest performance improvements come on the Terra Incognita dataset. The implementation details are described in the Supplementary.

### 5.3. Ablation Study and Analysis

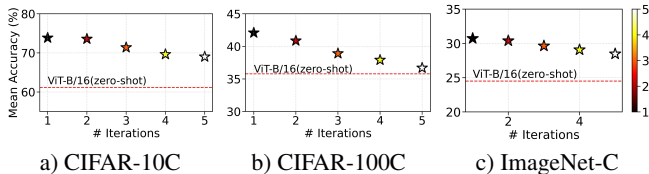


Figure 6. Analysis on increasing # iterations: Mean accuracy for # iterations, on each test batch, using a ViT-B/16 backbone.

**Adaptation for multiple iterations.** Here, we analyze adaptation for multiple iterations on a single batch, shown in Figure 6, using the ViT-B/16 backbone. Continuous adaptation of LN parameters, which normalize along the features of a single sample, can lead to overfitting as it fits to the noise patterns of the batch, ultimately degrading generalization to other domains. This could also lead to a decline in the loss of CLIP pre-trained knowledge. In the Supplementary, we report the post-adaptation results back on the source test sets - CIFAR10 and CIFAR100 to evaluate *catastrophic forgetting*. Our approach outperforms zero-shot CLIP, with a smaller decline in mean accuracy—especially on CIFAR-10C and ImageNet-C—showing that our loss components improve robustness under challenging conditions.

Backbone (ViT-B/16)	CIFAR-10C	CIFAR-100C	ImageNet-C
$\mathcal{L}_{ent}$	60.65	38.17	24.03
$\mathcal{L}_{pm}$	61.23	36.63	22.83
$\mathcal{L}_{sp}$	73.16	41.36	30.05
$\mathcal{L}_{ent} + \mathcal{L}_{pm}$	62.60	39.32	25.21
$\mathcal{L}_{ent} + 0.1 * (\mathcal{L}_{pm} + \mathcal{L}_{sp})$	71.90	41.88	30.24
$\mathcal{L}_{ent} + 0.5 * (\mathcal{L}_{pm} + \mathcal{L}_{sp})$	73.70	41.98	30.44
$\mathcal{L}_{ent} + \mathcal{L}_{pm} + \mathcal{L}_{sp}$	<b>73.85</b>	<b>42.09</b>	<b>30.72</b>

Table 3. Ablation on loss components - Mean accuracy (in %).

**Ablation on loss components.** In Table 3, we ablate the loss components by taking their different combinations using ViT-B/16. The task-wise results are reported in the Supplementary. We observe that the addition of  $\mathcal{L}_{pm}$  and  $\mathcal{L}_{sp}$  largely improve model performance than entropy minimization via  $\mathcal{L}_{ent}$ . In fact, the addition of  $\mathcal{L}_{sp}$  brings larger improvements, proving that  $f_{vis}$  produces discriminative features. Interestingly, using just  $\mathcal{L}_{ent}$  achieves better or comparable accuracy than zero-shot CLIP, as the encoders work in synergy while adapting to the domain.

**Low batch size setting.** In Eq 3, the prototype of each class can be affected by the batch size, with a lower size indicating the absence of a few classes. In Figure 7, we illustrate the mean accuracies on the benchmark datasets. As seen, BATCLIP still outperforms or performs comparably to TPT and VTE in low batch size settings. Since TTA happens at the batch-level of a specific domain, the prototypes are computed with the available pseudo-labels, aiding in the continual learning of the feature space as new batches come.

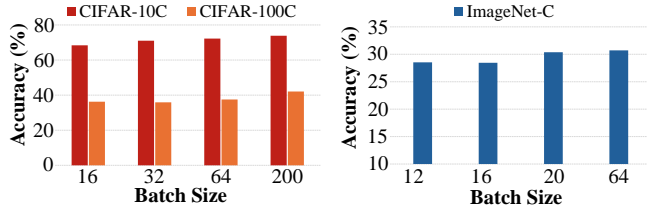


Figure 7. Ablation on low batch size - CIFAR-10C and CIFAR-100C (left) and ImageNet-C (right) using a ViT-B/16 backbone.

Dataset	ZS	TPT	VTE	Ours
CIFAR-10C	75.84	77.75	75.32	84.74
CIFAR-100C	47.82	49.62	48.53	49.25
ImageNet-C	39.55	40.96	40.55	42.84

(a) Mean acc. w/ a ViT-L/14.

Dataset	TENT	RPL	RoTTA	SAR	Ours
ImageNet-C	40.62	40.00	39.76	42.10	<b>42.84</b>

(b) TTA baselines vs ours w/ ViT-L/14.

Table 4. Ablation on a larger backbone (ViT-L/14) - Mean accuracy (in %)

**Extension to larger backbones.** We run BATCLIP for a larger backbone like ViT-L/14 and report the results in Table 4. *The key advantage lies in the projection matching loss ( $\mathcal{L}_{pm}$ ) which updates the text encoder to produce more image-aware text features—an aspect missing in other state-of-the-art TTA baselines.*

**Computational efficiency.** Due to an additional text encoder update, BATCLIP updates  $\sim 0.044\%$  of all CLIP parameters, with a ViT-B/16 backbone, as opposed to  $\sim 0.026\%$  in other TTA baselines. Though the increase is marginal, this leads to superior performances as adaptation of the text encoder produces input-aware CLIP text features, aligning better with the image features. On an NVIDIA RTX A5000 GPU, it takes 0.2s/batch on ImageNet-C with a batch size of 64, compared to 2.34s for WATT [36]. Also, WATT adapts per template (for several iterations), making it expensive every time. BATCLIP achieves faster on-the-fly adaptation rates and is favorable for real-time deployment.

## 6. Conclusion

In this work, we propose BATCLIP, a *bimodal online* test-time adaptation framework for CLIP aimed at handling diverse image corruptions simulating real-time environments. Our in-depth analysis of CLIP’s zero-shot performance under increasing corruption severity reveals significant shortcomings in generalization, highlighting the need for effective adaptation. Although prior work on TTA for CLIP has predominantly been *unimodal* focusing on prompt-tuning or prompt ensemble with no model updates, BATCLIP, through synergistic CLIP encoder updates, encourages learning rich class-separated visual features via vision encoder updates and strengthens alignment between the image class prototype and corresponding text feature via text encoder updates. Empirical studies, including ablations, show robust performance gains over all baselines on benchmark corruption and domain generalization datasets.

## References

- [1] Eduardo Arnold, Omar Y Al-Jarrah, Mehrdad Dianati, Saber Fallah, David Oxtoby, and Alex Mouzakitis. A survey on 3d object detection methods for autonomous driving applications. *IEEE Transactions on Intelligent Transportation Systems*, 20(10):3782–3795, 2019. 1
- [2] Hanoona Bangalath, Muhammad Maaz, Muhammad Uzair Khattak, Salman H Khan, and Fahad Shahbaz Khan. Bridging the gap between object and image-level representations for open-vocabulary detection. *Advances in Neural Information Processing Systems*, 35:33781–33794, 2022. 1
- [3] Sara Beery, Grant Van Horn, and Pietro Perona. Recognition in terra incognita. In *Proceedings of the European conference on computer vision (ECCV)*, pages 456–473, 2018. 2, 1
- [4] Dian Chen, Dequan Wang, Trevor Darrell, and Sayna Ebrahimi. Contrastive test-time adaptation. In *Proceedings of the IEEE/CVF Conference on Computer Vision and Pattern Recognition*, pages 295–305, 2022. 1, 2
- [5] Hanting Chen, Yunhe Wang, Tianyu Guo, Chang Xu, Yiping Deng, Zhenhua Liu, Siwei Ma, Chunjing Xu, Chao Xu, and Wen Gao. Pre-trained image processing transformer. In *Proceedings of the IEEE/CVF Conference on Computer Vision and Pattern Recognition*, pages 12299–12310, 2021. 3
- [6] Sungha Choi, Seunghan Yang, Seokeon Choi, and Sung-rack Yun. Improving test-time adaptation via shift-agnostic weight regularization and nearest source prototypes. In *European Conference on Computer Vision*, pages 440–458. Springer, 2022. 2
- [7] Marco Cuturi. Sinkhorn distances: Lightspeed computation of optimal transport. *Advances in neural information processing systems*, 26, 2013. 3
- [8] Jia Deng, Wei Dong, Richard Socher, Li-Jia Li, Kai Li, and Li Fei-Fei. Imagenet: A large-scale hierarchical image database. In *2009 IEEE Conference on Computer Vision and Pattern Recognition*, pages 248–255. IEEE, 2009. 3, 1
- [9] Mario Döbler, Robert A Marsden, and Bin Yang. Robust mean teacher for continual and gradual test-time adaptation. In *Proceedings of the IEEE/CVF Conference on Computer Vision and Pattern Recognition*, pages 7704–7714, 2023. 1
- [10] Mario Döbler, Robert A Marsden, Tobias Raichle, and Bin Yang. A lost opportunity for vision-language models: A comparative study of online test-time adaptation for vision-language models. *ECCV Workshops*, 2024. 1, 2, 3, 4, 6
- [11] Alexey Dosovitskiy. An image is worth 16x16 words: Transformers for image recognition at scale. *arXiv preprint arXiv:2010.11929*, 2020. 1, 3, 2
- [12] Chen Fang, Ye Xu, and Daniel N Rockmore. Unbiased metric learning: On the utilization of multiple datasets and web images for softening bias. In *Proceedings of the IEEE international conference on computer vision*, pages 1657–1664, 2013. 2, 1
- [13] Ian J Goodfellow, Mehdi Mirza, Da Xiao, Aaron Courville, and Yoshua Bengio. An empirical investigation of catastrophic forgetting in gradient-based neural networks. *arXiv preprint arXiv:1312.6211*, 2013. 1, 3
- [14] Ishaan Gulrajani and David Lopez-Paz. In search of lost domain generalization. *arXiv preprint arXiv:2007.01434*, 2020. 2, 7, 1
- [15] Gustavo Adolfo Vargas Hakim, David Osowiecki, Mehrdad Noori, Milad Cheraghlikhani, Ali Bahri, Moslem Yazdanpanah, Ismail Ben Ayed, and Christian Desrosiers. Clipartt: Light-weight adaptation of clip to new domains at test time. *arXiv preprint arXiv:2405.00754*, 2024. 2, 3, 4
- [16] Xu Han, Zhengyan Zhang, Ning Ding, Yuxian Gu, Xiao Liu, Yuqi Huo, Jiezhong Qiu, Yuan Yao, Ao Zhang, Liang Zhang, et al. Pre-trained models: Past, present and future. *AI Open*, 2:225–250, 2021. 3
- [17] Kaiming He, Xiangyu Zhang, Shaoqing Ren, and Jian Sun. Deep residual learning for image recognition. In *Proceedings of the IEEE Conference on Computer Vision and Pattern Recognition*, pages 770–778, 2016. 1, 3
- [18] Dan Hendrycks and Thomas Dietterich. Benchmarking neural network robustness to common corruptions and perturbations. *arXiv preprint arXiv:1903.12261*, 2019. 2, 3, 1
- [19] Dan Hendrycks and Kevin Gimpel. Early methods for detecting adversarial images. *arXiv preprint arXiv:1608.00530*, 2016. 1
- [20] Yannis Kalantidis, Giorgos Tolias, et al. Label propagation for zero-shot classification with vision-language models. In *Proceedings of the IEEE/CVF Conference on Computer Vision and Pattern Recognition*, pages 23209–23218, 2024. 3
- [21] Adilbek Karmanov, Dayan Guan, Shijian Lu, Abdulmotaleb El Saddik, and Eric Xing. Efficient test-time adaptation of vision-language models. *The IEEE/CVF Conference on Computer Vision and Pattern Recognition*, 2024. 1, 3
- [22] Alex Krizhevsky, Geoffrey Hinton, et al. Learning multiple layers of features from tiny images. 2009. 1, 3
- [23] Alexey Kurakin, Ian Goodfellow, and Samy Bengio. Adversarial machine learning at scale. *arXiv preprint arXiv:1611.01236*, 2016. 5
- [24] Boyi Li, Kilian Q Weinberger, Serge Belongie, Vladlen Koltun, and René Ranftl. Language-driven semantic segmentation. *arXiv preprint arXiv:2201.03546*, 2022. 1
- [25] Da Li, Yongxin Yang, Yi-Zhe Song, and Timothy M Hospedales. Deeper, broader and artier domain generalization. In *Proceedings of the IEEE international conference on computer vision*, pages 5542–5550, 2017. 2, 1
- [26] Yanghao Li, Naiyan Wang, Jianping Shi, Jiaying Liu, and Xiaodi Hou. Revisiting batch normalization for practical domain adaptation. *arXiv preprint arXiv:1603.04779*, 2016. 6
- [27] Jiayi Lin and Shaogang Gong. Gridclip: One-stage object detection by grid-level clip representation learning. *arXiv preprint arXiv:2303.09252*, 2023. 1
- [28] Chang Liu, Yinpeng Dong, Wenzhao Xiang, Xiao Yang, Hang Su, Jun Zhu, Yuefeng Chen, Yuan He, Hui Xue, and Shibao Zheng. A comprehensive study on robustness of image classification models: Benchmarking and rethinking. *International Journal of Computer Vision*, pages 1–23, 2024. 1
- [29] Huaishao Luo, Junwei Bao, Youzheng Wu, Xiaodong He, and Tianrui Li. Segclip: Patch aggregation with learnable

- centers for open-vocabulary semantic segmentation. In *International Conference on Machine Learning*, pages 23033–23044. PMLR, 2023. 1
- [30] Xiaosong Ma, Jie Zhang, Song Guo, and Wenchao Xu. Swapprompt: Test-time prompt adaptation for vision-language models. *Advances in Neural Information Processing Systems*, 36, 2024. 3
- [31] Zheda Mai, Ruiwen Li, Jihwan Jeong, David Quispe, Hyunwoo Kim, and Scott Sanner. Online continual learning in image classification: An empirical survey. *Neurocomputing*, 469:28–51, 2022. 1
- [32] Ségolène Martin, Yunshi Huang, Fereshteh Shakeri, Jean-Christophe Pesquet, and Ismail Ben Ayed. Transductive zero-shot and few-shot clip. In *Proceedings of the IEEE/CVF Conference on Computer Vision and Pattern Recognition*, pages 28816–28826, 2024. 3
- [33] Jan Hendrik Metzen, Tim Genewein, Volker Fischer, and Bastian Bischoff. On detecting adversarial perturbations. In *International Conference on Learning Representations*, 2017. 1
- [34] Shambhavi Mishra, Julio Silva-Rodríguez, Ismail Ben Ayed, Marco Pedersoli, and Jose Dolz. Words matter: Leveraging individual text embeddings for code generation in clip test-time adaptation. *arXiv preprint arXiv:2411.17002*, 2024. 2, 3, 4
- [35] Shuaicheng Niu, Jiayang Wu, Yifan Zhang, Zhiqian Wen, Yaofo Chen, Peilin Zhao, and Mingkui Tan. Towards stable test-time adaptation in dynamic wild world. In *International Conference on Machine Learning*, pages 16888–16905. PMLR, 2022. 1, 2, 3, 6
- [36] David Osowiechi, Mehrdad Noori, Gustavo Adolfo Vargas Hakim, Moslem Yazdanpanah, Ali Bahri, Milad Cheraghali, Sahar Dastani, Farzad Beizaei, Ismail Ben Ayed, and Christian Desrosiers. Watt: Weight average test-time adaption of clip. *arXiv preprint arXiv:2406.13875*, 2024. 2, 3, 4, 6, 8, 1
- [37] Nicolas Papernot, Patrick McDaniel, Xi Wu, Somesh Jha, and Ananthram Swami. Distillation as a defense to adversarial perturbations against deep neural networks. In *2016 IEEE symposium on security and privacy (SP)*, pages 582–597. IEEE, 2016. 1
- [38] Alec Radford, Jong Wook Kim, Chris Hallacy, Aditya Ramesh, Gabriel Goh, Sandhini Agarwal, Girish Sastry, Amanda Askell, Pamela Mishkin, Jack Clark, et al. Learning transferable visual models from natural language supervision. In *International Conference on Machine Learning*, pages 8748–8763. PMLR, 2021. 1, 2
- [39] Aditya Ramesh, Prafulla Dhariwal, Alex Nichol, Casey Chu, and Mark Chen. Hierarchical text-conditional image generation with clip latents. *arXiv preprint arXiv:2204.06125*, 1(2):3, 2022. 1
- [40] Robin Rombach, Andreas Blattmann, Dominik Lorenz, Patrick Esser, and Björn Ommer. High-resolution image synthesis with latent diffusion models. In *Proceedings of the IEEE/CVF conference on computer vision and pattern recognition*, pages 10684–10695, 2022. 1
- [41] Evgenia Rusak, Steffen Schneider, George Pachitariu, Luisa Eck, Peter Gehler, Oliver Bringmann, Wieland Brendel, and Matthias Bethge. If your data distribution shifts, use self-learning. *arXiv preprint arXiv:2104.12928*, 2021. 1, 2, 6
- [42] Christos Sakaridis, Dengxin Dai, and Luc Van Gool. Acdc: The adverse conditions dataset with correspondences for semantic driving scene understanding. In *Proceedings of the IEEE/CVF International Conference on Computer Vision*, pages 10765–10775, 2021. 1
- [43] Steffen Schneider, Evgenia Rusak, Luisa Eck, Oliver Bringmann, Wieland Brendel, and Matthias Bethge. Improving robustness against common corruptions by covariate shift adaptation. *Advances in Neural Information Processing Systems*, 33:11539–11551, 2020. 1, 2
- [44] Claude Elwood Shannon. A mathematical theory of communication. *The Bell system technical journal*, 27(3):379–423, 1948. 2, 6
- [45] Manli Shu, Weili Nie, De-An Huang, Zhiding Yu, Tom Goldstein, Anima Anandkumar, and Chaowei Xiao. Test-time prompt tuning for zero-shot generalization in vision-language models. *Advances in Neural Information Processing Systems*, 35:14274–14289, 2022. 1, 2, 3, 4, 6
- [46] Jake Snell, Kevin Swersky, and Richard Zemel. Prototypical networks for few-shot learning. *Advances in Neural Information Processing Systems*, 30, 2017. 5
- [47] Adarsh Subbaswamy, Roy Adams, and Suchi Saria. Evaluating model robustness and stability to dataset shift. In *International Conference on Artificial Intelligence and Statistics*, pages 2611–2619. PMLR, 2021. 1
- [48] Yu Sun, Xiaolong Wang, Zhuang Liu, John Miller, Alexei Efros, and Moritz Hardt. Test-time training with self-supervision for generalization under distribution shifts. In *International Conference on Machine Learning*, pages 9229–9248. PMLR, 2020. 1, 2
- [49] Laurens Van der Maaten and Geoffrey Hinton. Visualizing data using t-sne. *Journal of Machine Learning Research*, 9(11), 2008. 6, 7
- [50] A Vaswani. Attention is all you need. *Advances in Neural Information Processing Systems*, 2017. 4
- [51] Hemanth Venkateswara, Jose Eusebio, Shayok Chakraborty, and Sethuraman Panchanathan. Deep hashing network for unsupervised domain adaptation. In *Proceedings of the IEEE conference on computer vision and pattern recognition*, pages 5018–5027, 2017. 2, 1
- [52] Yael Vinker, Ehsan Pajouheshgar, Jessica Y Bo, Roman Christian Bachmann, Amit Haim Bermano, Daniel Cohen-Or, Amir Zamir, and Ariel Shamir. Clipasso: Semantically-aware object sketching. *ACM Transactions on Graphics (TOG)*, 41(4):1–11, 2022. 1
- [53] Dequan Wang, Evan Shelhamer, Shaoteng Liu, Bruno Olshausen, and Trevor Darrell. Tent: Fully test-time adaptation by entropy minimization. In *International Conference on Learning Representations*, 2021. 1, 2, 3, 4, 6
- [54] Longhui Yuan, Binhui Xie, and Shuang Li. Robust test-time adaptation in dynamic scenarios. In *Proceedings of the IEEE/CVF Conference on Computer Vision and Pattern Recognition*, pages 15922–15932, 2023. 2, 6, 1
- [55] Maxime Zanella, Clément Fuchs, Christophe De Vleeschouwer, and Ismail Ben Ayed. Realistic

- test-time adaptation of vision-language models. *arXiv preprint arXiv:2501.03729*, 2025. 3, 6, 2
- [56] Maxime Zanella, Benoît Gérin, and Ismail Ayed. Boosting vision-language models with transduction. *Advances in Neural Information Processing Systems*, 37:62223–62256, 2025. 3
- [57] Marvin Zhang, Sergey Levine, and Chelsea Finn. Memo: Test time robustness via adaptation and augmentation. *Advances in Neural Information Processing Systems*, 35:38629–38642, 2022. 2
- [58] Bingchen Zhao, Haoqin Tu, Chen Wei, Jieru Mei, and Cihang Xie. Tuning layernorm in attention: Towards efficient multi-modal llm finetuning. *arXiv preprint arXiv:2312.11420*, 2023. 2, 6, 4
- [59] Shuai Zhao, Xiaohan Wang, Linchao Zhu, and Yi Yang. Test-time adaptation with clip reward for zero-shot generalization in vision-language models. *arXiv preprint arXiv:2305.18010*, 2023. 3
- [60] Kaiyang Zhou, Jingkang Yang, Chen Change Loy, and Ziwei Liu. Conditional prompt learning for vision-language models. In *Proceedings of the IEEE/CVF Conference on Computer Vision and Pattern Recognition*, pages 16816–16825, 2022. 1
- [61] Kaiyang Zhou, Jingkang Yang, Chen Change Loy, and Ziwei Liu. Learning to prompt for vision-language models. *International Journal of Computer Vision*, 130(9):2337–2348, 2022. 1, 3

# BATCLIP: Bimodal Online Test-Time Adaptation for CLIP

## Supplementary Material

In this work, we study the problem of **online** test-time adaptation (TTA) of CLIP [38] towards common image corruptions and propose improved schemes for increasing the robustness of CLIP. In addition, to demonstrate the broad impact of our proposed approach, we evaluate on common domain generalization datasets [14]-OfficeHome [51], PACS [25], VLCS [12], and Terra Incognita [3]. We put forward a *bimodal* domain adaptation scheme, at test-time, wherein we exploit the shared feature space of CLIP. In essence, leaning towards a more effective multimodal learning and adaptation method, we propose loss components that improve alignment between the class-specific visual prototype and corresponding text features via maximizing the projection. We also increase the cosine distance between the class prototypes to enhance discrimination between visual features. In this Supplementary, we provide additional insights and experimental results, that has been organized as follows,

1. Section 6.1 offers a detailed discussion of the standard common corruption datasets [18] used, supplemented with visual illustrations.
2. To ensure full transparency, we outline the implementation details of all the methods in Section 6.2, including those for prior TTA approaches [35, 41, 53, 54] adapted for CLIP. We also discuss details of the adapted version of WATT [36] - WATT-P\* and WATT-S\* for online TTA, and other details of experiments run on the domain generalization datasets.
3. Section 6.3 presents further results and analysis:
  - In subsection 6.3.1, we explore the limitations of zero-shot CLIP when using ViT-B/32 and ViT-L/14 backbones under increasing image corruption severity.
  - In Subsection 6.3.2, we report the main online TTA results on CIFAR-10C, CIFAR-100C, and ImageNet-C with a ViT-B/32 backbone.
  - We study the effect of different prompt templates on BATCLIP in Subsection 6.3.4. Subsection 6.3.5 discusses the ablation of  $\mathcal{L}_{pm}$  which is responsible for updating the text encoder.
  - In subsections 6.3.3 and 6.3.6, we present a detailed loss ablation study and the post-adaptation zero-shot generalization on source test sets, respectively — essentially evaluating *catastrophic forgetting* of BATCLIP.
  - Lastly, we include task-wise t-SNE visualizations in subsection 6.3.7 for CIFAR-10C and CIFAR-100C, comparing our method against zero-shot CLIP (ViT-B/16), to illustrate the effectiveness of BATCLIP.

### 6.1. Datasets

We employ the **CIFAR-10C**, **CIFAR-100C**, and **ImageNet-C** datasets, for our experiments, as introduced by [18]. Each dataset includes 15 distinct types of image corruptions, referred to as tasks in a test-time adaptation setting, applied to the test sets of CIFAR10, CIFAR100 [22], and ImageNet [8]. These corruptions are applied at 5 different severity levels, ranging from mild to severe. For each task, CIFAR-10C and CIFAR-100C contain 10,000 test samples, whereas ImageNet-C has 5000 samples.

The image corruptions are categorized into four primary groups: noise, blur, weather, and digital distortions. Noise-based corruptions include *Gaussian*, *Shot*, and *Impulse* noise, which introduce random pixel-level variations. The blur category encompasses *Defocus*, *Glass*, *Motion*, and *Zoom* blur effects, all of which simulate different types of distorted imagery. Weather-related corruptions, such as *Snow*, *Frost*, and *Fog*, replicate environmental conditions that obscure image details. Lastly, digital distortions include effects like *Brightness*, *Contrast*, *Elastic Transform*, *Pixelate*, and *JPEG* compression, which reflect various forms of post-processing or compression artifacts that degrade image quality.

These corruption types, as proposed by [18], provide a comprehensive framework for assessing model robustness, which has been and is still being studied [19, 28, 33, 37, 47]. Their ability to emulate real-world image degradation scenarios is advantageous, allowing for a more realistic evaluation of a model’s robustness. We provide corruption visualizations, via an image example, in Figure 8. We urge the readers to check out [18] for further inspection.



Figure 8. We provide visualizations of an image from ImageNet-C [18] for different corruption types, at an image severity level of 5.

## 6.2. Implementation Details

In this section, we summarize the implementation details of all the baseline methods that have been mentioned in the main paper, including ours. We build our approach on the standard benchmark code base<sup>2</sup> that also houses the hyperparameters and training details of all the prior TTA methods. CLIP-like models are used as provided by **OpenCLIP**. Only the vision encoder is updated for existing online TTA methods [35, 41, 53, 54] adopted for CLIP.

### 6.2.1. Experiments on CIFAR-10C, CIFAR-100C, and ImageNet-C

**BATCLIP (Ours)**: For domain-specific test adaptation, we conducted experiments using ViT-B/16 and ViT-B/32 [11] as the vision backbones. For CIFAR-10C, both the vision encoder ( $f_{vis}$ ) and text encoder ( $f_{txt}$ ) were updated using the AdamW optimizer with a learning rate of  $10^{-3}$ . Similarly, for CIFAR-100C and ImageNet-C, we employed the Adam optimizer and AdamW optimizer, respectively, with a learning rate of  $5 \times 10^{-4}$ . The batch size  $\mathcal{B}$  used was set to 200 for CIFAR-10C and CIFAR-100C, and 64 for ImageNet-C. Throughout, the prompt template is fixed to “a photo of a <CLS>.”.

**TENT [53]**: We follow all the hyperparameters that TENT provides in their official implementation<sup>3</sup>. To update the vision encoder, we use Adam as the optimizer with a learning rate of  $10^{-3}$  for CIFAR-10C and CIFAR-100C. For ImageNet-C, we update using SGD with a learning rate of  $25 \times 10^{-5}$ .

**RoTTA [54]**: For fairness, the batch sizes are set to 200 for the CIFAR datasets and 64 for ImageNet-C. The vision encoder is updated based on the Adam rule with a learning rate of  $10^{-3}$ . The capacity of the memory bank is set to 64, for all the datasets. Following the notations in the paper,  $\alpha = 0.05$ ,  $\delta = 0.1$ ,  $\nu = 0.001$ ,  $\lambda_\ell$  and  $\lambda_u = 1.0$ . We implement the details exactly as described in their main paper.

**RPL [41]**: We use an Adam optimizer with a learning rate of  $10^{-3}$  for CIFAR-10C and CIFAR-100C. For ImageNet-C, the update rule is SGD with a learning rate of  $5 \times 10^{-4}$ . To compute the generalized cross-entropy loss,  $q$  is set to 0.8 for all the datasets.

**SAR [35]**: The training details/hyperparameters for SAR are the same as RPL [41] for CIFAR-10 and CIFAR-100. For ImageNet-C, the learning rate is set to  $25 \times 10^{-5}$  with an SGD update rule. The entropy threshold  $E_0$  is  $0.4 \times \ln(C)$ , where  $C$  is the number of classes.  $\rho$  is set to a default of 0.05. The moving average factor is 0.9 for  $e_m$  and  $e_0$  is set to 0.2. All parameters are the same as in [35].

**TPT [45]**: For each test image, 63 augmentations are generated based on random resized crops, yielding a batch of 64 images, in addition to the original test image. The

prompt/context vectors are initialized based on “a photo of a <CLS>.” and tokenized using pre-trained CLIP weights. The confidence threshold is set to 10% *i.e.*, the marginal entropy over the 10% confident samples is minimized. For all the datasets, we follow their core implementation and optimize the prompt vectors using an AdamW optimizer with a learning rate of  $5 \times 10^{-3}$ .

**VTE [10]**: In VTE, an ensemble of different prompt templates is considered based on the idea of [38]. An example of templates includes “a photo of a <CLS>.”, “a sketch of a <CLS>.”, “a painting of a <CLS>.”, etc. The prompt templates are then averaged. On the vision side, similar to TPT [45], a batch of random augmentation is created for a test image with no model updates.

**WATT-P\* and WATT-S\* [36]**: The two original variants of WATT [36] were proposed with weight-averaging of adapted weights from multiple prompt templates. Additionally, for each test batch, adaptation was performed over multiple iterations. To fit our online TTA scheme, we reduced the number of iterations to a single step for each prompt template and reset CLIP parameters only after a domain. However, this is still not fully online, as *training* is performed on the test batch using 8 selected prompt templates: “a photo of a <CLS>”, “itap of a <CLS>”, “a bad photo of the <CLS>”, “a origami <CLS>”, “a photo of the large <CLS>”, “a <CLS> in a video game”, “art of the <CLS>”, and “a photo of the small <CLS>”. As they report performance on CIFAR-10C and CIFAR-100C only, we follow their original implementation details. For experiments using WATT-S\*, we set a batch size of 200 (for a fair comparison to other baselines) and a learning rate of  $10^{-3}$  using an Adam optimizer. For WATT-P\*, a learning rate of  $10^{-4}$  is used with the same batch size.

**StatA [55]**: We adopt the original hyperparameter settings of StatA for online TTA in our reported ImageNet experiments and apply them to ImageNet-C. To control the effective number of correlated classes in a test batch, we set  $\gamma$  to 0.1 (low correlation) and -1 (separate, sequential). The default prompt template is “a photo of a <CLS>.”

### 6.2.2. Experiments on Domain Generalization Datasets

We evaluate **BATCLIP** on standard domain generalization datasets [14]. For a fair comparison, as reported in WATT [36], we use a batch size of 128 for all the online TTA experiments on VLCS, PACS, and Office Home. We use an AdamW optimizer for model updates using **BATCLIP** with learning rates of  $5 \times 10^{-4}$ ,  $10^{-3}$ , and  $5 \times 10^{-3}$  for Office-Home, PACS, and VLCS, respectively. We use the same learning settings for TENT, WATT-S\*, and WATT-P\*, as in WATT [36]. In addition to the mentioned datasets, we also run experiments on the Terra Incognita dataset and optimize using an AdamW optimizer with a learning rate of  $5 \times 10^{-4}$  and a batch size of 256.

<sup>2</sup><https://github.com/mariodoebler/test-time-adaptation/tree/main>

<sup>3</sup><https://github.com/DequanWang/tent>

	<u>CLIP (ViT-B/16)</u>	<u>VTE</u>	<u>TPT</u>	<u>Ours</u>
	GT: valley 😊 Prediction: valley	GT: valley 😞 Prediction: alp	GT: valley 😞 Prediction: CRT screen	GT: valley 😊 Prediction: valley
	GT: hook skirt 😞 Prediction: overskirt	GT: hook skirt 😞 Prediction: television	GT: hook skirt 😊 Prediction: hook skirt	GT: hook skirt 😊 Prediction: hook skirt
	GT: stage 😞 Prediction: front curtain	GT: stage 😞 Prediction: television	GT: stage 😞 Prediction: projector	GT: stage 😊 Prediction: stage
	GT: orangutan 😊 Prediction: orangutan	GT: orangutan 😞 Prediction: gorilla	GT: orangutan 😊 Prediction: orangutan	GT: orangutan 😊 Prediction: orangutan

Figure 9. Comparison of classification predictions across various methods (Zero-shot CLIP (ViT-B/16), VTE [10], TPT [45], and Ours) on ImageNet-C samples with *Gaussian* noise. Each row illustrates an example, displaying the ground truth (GT) label alongside the predictions from each method. Correct predictions are highlighted in green, while incorrect ones are marked in red. Our approach demonstrates enhanced robustness and higher accuracy, especially in challenging image corruption conditions.

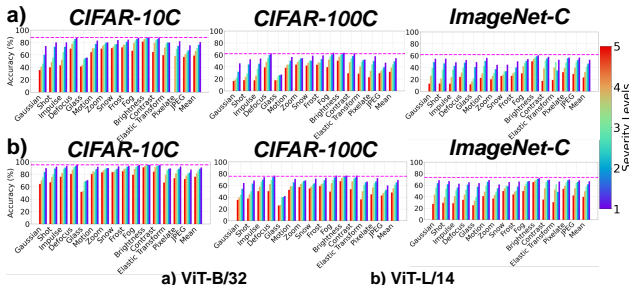


Figure 10. Task-wise mean accuracy (%) of zero-shot CLIP across different corruption severity levels. [Top]: ViT-B/32 backbone. [Bottom]: ViT-L/14 backbone. The **dashed lines** indicate the performance of zero-shot CLIP (w/ respective visual backbones) on the corresponding source datasets.

### 6.3. Additional Results

In the following subsections, we provide additional results and discussions.

#### 6.3.1. Zero-shot performance analysis of ViT-B/32 and ViT-L/14

In the main paper, we analyze and evaluate the zero-shot performance of ResNet-101 (RN101) [17] and ViT-B/16

[11] and conclude that such CLIP backbones are extremely sensitive, in terms of classification accuracy, to increasing severity levels of image corruption. This could be a major concern in situations involving real-time deployment of CLIP. Here, we present a similar analysis in Figure 10, using ViT-B/32 and ViT-L/14 as backbones. Our analysis, from the main paper, carries forward. To summarise, irrespective of the CLIP visual backbone, the robustness towards image corruption is limited. The classification performance degrades with an increase in the severity of corruption in an image.

#### 6.3.2. Online TTA results using a ViT-B/32 backbone

In the main paper, we had presented the online TTA results on CIFAR-10C, CIFAR-100C, and ImageNet-C, using a ViT-B/16 backbone. In Table 5, we provide results using a ViT-B/32 backbone. Across all the datasets, we see that BATCLIP achieves the best or comparable performance against all the baseline approaches.

#### 6.3.3. Detailed results from the loss ablation study

In the main paper, we provide ablation of loss components and their combinations *i.e.*, the mean accuracy across all the tasks for ViT-B/16 on the benchmark corruption datasets. Here, we provide additional task-wise accuracy in Table 6.

Method	Venue	Corruption															Mean	
		Gaussian	Shot	Impulse	Defocus	Glass	Motion	Zoom	Snow	Frost	Fog	Brightness	Contrast	Elastic	Pixellate	JPEG		
CIFAR-10C	ZS	ICLR'21	35.47	39.94	43.23	69.95	41.43	64.50	70.13	70.85	72.33	66.66	81.37	64.57	59.69	48.28	56.62	59.00
	TENT	ICLR'21	20.09	23.45	34.47	69.85	23.01	39.79	60.35	76.83	77.49	76.07	<b>88.88</b>	<b>81.38</b>	65.35	57.01	51.19	56.35
	RoTTA	CVPR'23	36.55	40.91	43.99	70.03	42.45	64.52	70.08	71.23	72.68	67.31	81.92	64.99	60.33	49.40	57.11	59.57
	RPL	arXiv	15.89	19.08	34.04	<b>77.84</b>	18.72	41.22	62.39	78.17	78.86	<b>76.31</b>	88.83	81.15	68.98	54.19	51.91	56.51
	SAR	ICML'22	50.28	54.12	49.65	73.08	51.98	71.17	74.65	73.73	75.22	70.99	84.25	72.08	63.93	51.57	60.32	65.13
	TPT	NeurIPS'22	43.11	46.53	48.29	71.31	47.80	66.89	71.96	74.00	76.00	68.81	84.12	66.35	63.86	51.86	58.01	62.59
	VTE	ECCV-W'24	47.59	50.18	<b>53.15</b>	71.39	53.86	67.92	72.90	76.37	76.30	70.78	83.27	61.07	69.00	58.57	61.14	64.90
	WATT-P*	NeurIPS'24	43.64	47.1	45.97	74.98	48.04	70.42	74.74	76.1	76.86	71.85	85.15	70.36	64.6	56.0	60.37	64.41
	WATT-S*	NeurIPS'24	<b>56.38</b>	<b>58.08</b>	52.48	78.07	<b>58.29</b>	<b>76.42</b>	<b>79.16</b>	<b>78.9</b>	<b>79.71</b>	76.76	87.19	76.49	<b>70.35</b>	<b>64.11</b>	<b>65.05</b>	<b>70.49</b>
	Ours		52.39	55.99	52.54	76.79	54.04	74.90	75.79	77.67	79.10	75.31	86.33	77.34	67.41	57.06	61.29	68.26
CIFAR-100C	ZS	ICLR'21	16.23	17.83	17.57	39.07	17.63	38.55	43.81	42.32	43.46	39.71	50.32	29.34	28.74	22.85	29.42	31.79
	TENT	ICLR'21	5.53	7.64	6.85	<b>49.60</b>	4.47	48.45	52.35	49.77	26.77	37.50	63.05	<b>50.53</b>	13.89	27.00	30.80	31.61
	RoTTA	CVPR'23	16.63	18.25	17.78	38.62	17.76	38.38	43.52	42.39	43.41	39.37	50.60	28.85	28.89	23.50	29.65	31.84
	RPL	arXiv	4.50	5.80	9.61	50.26	4.43	<b>48.88</b>	<b>52.61</b>	<b>50.27</b>	22.36	25.34	<b>63.36</b>	50.31	9.10	18.65	<b>34.53</b>	30.00
	SAR	ICML'22	<b>24.63</b>	<b>27.14</b>	21.25	44.57	22.98	<b>43.95</b>	48.40	48.01	<b>47.76</b>	44.85	57.76	42.11	32.69	<b>28.02</b>	<b>33.08</b>	<b>37.81</b>
	TPT	NeurIPS'22	16.08	17.65	17.54	39.21	19.47	38.91	44.01	43.45	44.46	40.15	50.93	27.77	30.91	23.36	29.55	32.23
	VTE	ECCV-W'24	16.84	18.33	18.94	39.63	22.88	39.13	43.80	44.56	44.88	39.21	49.37	28.37	34.13	26.87	30.12	33.14
	WATT-P*	NeurIPS'24	15.55	17.02	16.16	40.25	16.16	38.74	43.6	42.49	43.51	39.39	51.17	31.85	28.35	23.94	29.74	31.86
	WATT-S*	NeurIPS'24	16.22	17.72	16.85	41.54	17.04	39.66	44.55	43.33	44.26	40.26	52.13	33.13	29.34	24.65	30.39	32.73
	Ours		21.35	24.71	<b>22.32</b>	46.26	<b>23.07</b>	44.64	50.12	47.23	46.88	<b>44.92</b>	58.55	38.52	<b>34.56</b>	27.73	33.19	37.60
ImageNet-C	ZS	ICLR'21	12.88	13.04	12.90	24.42	11.86	22.72	20.20	25.70	25.84	30.28	50.54	17.32	18.96	32.20	29.12	23.20
	TENT	ICLR'21	9.18	8.50	10.42	<b>26.02</b>	15.72	26.06	21.64	27.12	26.18	31.60	50.58	22.28	20.12	34.06	31.30	24.05
	RoTTA	CVPR'23	13.10	13.30	13.02	24.48	11.96	22.86	20.28	26.06	26.06	30.24	50.46	17.34	19.16	32.44	29.18	23.33
	RPL	arXiv	11.68	10.98	12.10	25.68	13.24	23.98	20.84	26.32	26.12	30.86	50.62	19.30	19.48	33.14	29.92	23.62
	SAR	ICML'22	<b>19.82</b>	<b>20.36</b>	<b>20.92</b>	25.78	20.40	28.34	23.10	28.12	<b>28.38</b>	34.74	51.10	<b>24.60</b>	24.38	<b>36.54</b>	34.40	<b>28.07</b>
	TPT	NeurIPS'22	12.04	12.64	12.52	25.38	12.28	22.68	20.78	26.36	26.64	30.78	51.02	16.50	19.90	33.62	30.62	23.58
	VTE	ECCV-W'24	11.96	12.32	13.44	25.06	11.70	22.58	22.40	27.38	27.02	32.28	<b>51.52</b>	16.84	19.94	34.80	32.82	24.14
	StatA ( $\gamma=0.1$ )	CVPR'25	11.57	12.28	11.74	21.91	10.91	20.43	18.87	24.04	25.0	29.12	49.21	16.02	18.87	29.15	26.72	21.73
	StatA ( $\gamma=-1$ )	CVPR'25	12.52	13.10	12.74	22.43	11.39	21.17	19.61	24.37	25.60	29.44	49.89	17.71	19.21	29.87	27.52	22.44
	Ours		16.84	18.20	16.10	25.04	<b>20.90</b>	<b>28.90</b>	<b>25.24</b>	<b>29.42</b>	27.18	<b>36.02</b>	50.18	17.66	<b>27.68</b>	36.20	<b>35.42</b>	27.39

Table 5. Mean accuracy (%) on CIFAR-10C, CIFAR-100C, and ImageNet-C - TTA mean accuracy of the 15 corruptions (tasks) at a severity level of 5, using ViT-B/32.

The addition of loss components  $\mathcal{L}_{pm}$  and  $\mathcal{L}_{sp}$  help CLIP in adapting its feature space to a specific domain/corruption.

### 6.3.4. Effect of different prompt templates

In Table , we show results with “relevant” prompt templates to show the independence of such prompt selection, at test-time. As seen, the performance gain over zero-shot ViT-B/32 is fairly large for all the prompt templates. Though TPT [45] fine-tunes a pre-trained prompt on each image, and VTE [10] uses an ensemble of prompts, our method is agnostic to the prompt template being used, making it favorable for real-time usage.

In all of our prior experiments, we use a generic prompt template “a photo of a <CLS>.” for all of the datasets and methods. Here, we replace this with “relevant” prompt templates to show the independence of such a prompt selection, at test-time, and report the results in Table 9. As seen, the performance gain over zero-shot ViT-B/32 is fairly large for all the prompt templates. Though TPT [45] fine-tunes a pre-trained prompt on each test image, and VTE [10] uses an ensemble of prompts, our method is agnostic to the prompt template being used, making it favorable for real-time deployment.

### 6.3.5. Impact of bimodal adaptation

To show the effectiveness of *bimodal* adaptation, we ablate  $\mathcal{L}_{pm}$ , which is responsible for updating the text encoder  $f_{txt}$ . We report the results in Table 10. We see a drop in accuracy when  $f_{txt}$  is “frozen” i.e., when  $\mathcal{L}_{pm}$  isn’t used, necessitating the need for *bimodal* adaptation of CLIP encoders.

### 6.3.6. Post-adaptation results on source test sets

Thanks to the natural language supervision and also due to the pre-training on large amounts of (image, text) pairs, CLIP has shown strong generalization capabilities. However, for an efficient adaptation to a downstream task, fine-tuning the full model is infeasible due to large model updates. The primary reason is the loss of useful pre-trained knowledge of CLIP, which could eventually lead to overfitting to a downstream task. However, for attention-based models, tuned for multimodal tasks, [58] show that tuning the *LayerNorm* parameters leads to strong results. Inspired by [58], in our *bimodal* test-adaptation scheme, we update the *LayerNorm* parameters of both CLIP encoders, to a specific corruption task, which makes it parametric-efficient. We perform a single-domain TTA or adapt CLIP, at test-time, to a single domain only and then reset the parameters. Now, with continual adaptation to a certain corruption task,

Method		Gaussian	Shot	Impulse	Defocus	Glass	Motion	Zoom	Snow	Frost	Fog	Brightness	Contrast	Elastic	Pixelate	JPEG	Mean
CIFAR-10C	ViT-B/16																
	$\mathcal{L}_{ent}$	14.62	17.29	49.25	<b>81.06</b>	20.23	74.27	81.10	<b>84.25</b>	81.93	<b>80.93</b>	<b>91.86</b>	78.92	53.09	51.18	49.79	60.65
	$\mathcal{L}_{pm}$	41.82	45.66	52.88	70.13	39.29	66.61	71.27	71.49	74.71	69.20	80.98	72.89	55.58	55.55	50.44	61.23
	$\mathcal{L}_{sp}$	62.47	65.43	63.41	79.96	52.73	80.02	81.38	82.35	83.44	80.46	88.85	81.22	67.77	60.52	67.74	73.16
	$\mathcal{L}_{ent}+\mathcal{L}_{pm}$	16.58	19.89	42.69	79.45	23.41	77.03	80.95	81.74	78.45	80.66	90.52	<b>82.55</b>	62.56	<b>64.35</b>	58.16	62.60
	$\mathcal{L}_{ent} + 0.1 * (\mathcal{L}_{pm} + \mathcal{L}_{sp})$	44.92	51.41	63.30	80.65	50.79	79.83	83.13	83.59	83.89	81.91	89.56	83.16	67.78	66.69	67.87	71.90
	$\mathcal{L}_{ent} + 0.5 * (\mathcal{L}_{pm} + \mathcal{L}_{sp})$	58.81	63.85	65.99	80.26	53.90	80.30	82.30	83.08	84.04	81.66	89.19	82.67	68.29	62.70	68.52	73.70
	$\mathcal{L}_{ent}+\mathcal{L}_{pm}+\mathcal{L}_{sp}$	<b>61.13</b>	<b>64.09</b>	<b>65.76</b>	80.51	<b>54.96</b>	<b>80.65</b>	<b>81.94</b>	83.04	<b>84.19</b>	80.84	88.95	82.15	<b>69.16</b>	62.68	<b>67.64</b>	<b>73.85</b>
CIFAR-100C	ViT-B/16																
	$\mathcal{L}_{ent}$	7.71	10.05	11.52	49.42	12.49	<b>49.36</b>	53.79	<b>54.11</b>	50.76	<b>49.92</b>	<b>64.32</b>	<b>47.07</b>	33.40	<b>38.63</b>	<b>39.95</b>	38.17
	$\mathcal{L}_{pm}$	19.88	24.06	21.26	45.57	22.66	43.66	49.37	46.05	45.96	43.69	57.76	37.33	33.66	25.85	32.65	36.63
	$\mathcal{L}_{sp}$	24.69	27.28	33.62	49.08	25.29	47.84	53.86	51.70	50.93	46.93	62.57	44.76	33.88	31.89	36.05	41.36
	$\mathcal{L}_{ent}+\mathcal{L}_{pm}$	12.26	12.62	13.14	48.90	26.22	48.99	53.10	53.10	<b>52.43</b>	49.44	63.36	46.78	33.27	37.77	38.36	39.32
	$\mathcal{L}_{ent} + 0.1 * (\mathcal{L}_{pm} + \mathcal{L}_{sp})$	24.99	27.10	32.95	49.92	25.91	48.42	54.43	52.87	51.57	47.70	63.68	45.25	39.74	31.58	37.16	41.88
	$\mathcal{L}_{ent} + 0.5 * (\mathcal{L}_{pm} + \mathcal{L}_{sp})$	25.24	27.59	33.41	50.05	25.73	48.55	54.44	52.85	51.80	47.81	63.75	45.08	34.63	31.67	37.17	41.98
	$\mathcal{L}_{ent}+\mathcal{L}_{pm}+\mathcal{L}_{sp}$	<b>24.91</b>	<b>27.73</b>	<b>33.66</b>	<b>50.11</b>	<b>26.27</b>	48.49	<b>54.85</b>	52.35	51.62	48.38	63.27	45.21	<b>34.74</b>	32.38	37.31	<b>42.09</b>
ImageNet-C	ViT-B/16																
	$\mathcal{L}_{ent}$	0.90	1.06	1.16	<b>29.12</b>	13.02	<b>32.14</b>	27.34	35.32	11.14	40.92	<b>56.90</b>	23.78	7.78	39.62	40.22	24.03
	$\mathcal{L}_{pm}$	10.20	11.40	10.74	19.56	15.18	20.06	19.28	27.66	29.72	34.10	53.50	22.66	13.80	24.38	30.26	22.83
	$\mathcal{L}_{sp}$	19.32	20.98	19.26	25.90	21.22	30.06	28.56	35.22	31.34	40.36	55.20	25.64	23.68	36.90	37.18	30.05
	$\mathcal{L}_{ent}+\mathcal{L}_{pm}$	0.90	1.16	1.30	28.90	17.04	31.56	26.24	36.26	12.22	<b>42.12</b>	57.92	<b>30.34</b>	10.36	<b>40.66</b>	<b>41.20</b>	25.21
	$\mathcal{L}_{ent} + 0.1 * (\mathcal{L}_{pm} + \mathcal{L}_{sp})$	19.48	21.14	19.16	26.80	20.70	29.80	29.32	35.92	30.68	41.04	55.80	25.66	22.50	37.68	37.92	30.25
	$\mathcal{L}_{ent} + 0.5 * (\mathcal{L}_{pm} + \mathcal{L}_{sp})$	19.56	21.38	19.16	26.96	21.26	30.06	29.24	35.92	31.26	41.34	56.32	25.74	22.58	37.94	37.92	30.44
	$\mathcal{L}_{ent}+\mathcal{L}_{pm}+\mathcal{L}_{sp}$	<b>19.32</b>	<b>21.38</b>	<b>19.60</b>	26.58	<b>21.94</b>	30.88	<b>29.02</b>	<b>36.48</b>	32.00	40.98	56.72	26.14	<b>23.74</b>	37.68	38.34	<b>30.72</b>

Table 6. Task-wise loss ablation results (accuracy) on CIFAR-10C, CIFAR-100C, and ImageNet-C.

Method	Gaussian	Shot	Impulse	Defocus	Glass	Motion	Zoom	Snow	Frost	Fog	Brightness	Contrast	Elastic	Pixelate	JPEG	Zero-Shot
ViT-B/16																90.1
Ours	84.51	84.29	88.69	88.48	86.44	86.46	87.04	91.38	91.01	90.22	90.87	88.12	88.13	74.74	87.48	87.19 (mean)
ViT-B/32																88.3
Ours	67.41	68.28	84.23	80.50	75.37	79.75	78.55	87.67	86.36	85.83	90.04	80.89	81.56	82.74	82.36	80.77 (mean)

Table 7. Zero-shot performance on CIFAR10 (source) after adaptation of BATCLIP on a task.

Method	Gaussian	Shot	Impulse	Defocus	Glass	Motion	Zoom	Snow	Frost	Fog	Brightness	Contrast	Elastic	Pixelate	JPEG	Zero-Shot
ViT-B/16																66.6
Ours	67.09	67.12	67.08	70.31	63.70	66.83	70.12	70.10	68.19	69.55	71.05	66.49	65.13	59.98	67.60	67.36 (mean)
ViT-B/32																62.3
Ours	45.99	46.90	60.86	63.62	57.73	59.59	61.66	66.21	61.50	63.61	66.39	57.05	62.13	62.82	65.37	60.09 (mean)

Table 8. Zero-shot performance on CIFAR100 (source) after adaptation of BATCLIP on a task.

Prompt Template	CIFAR-10C	CIFAR-100C	ImageNet-C
"a low contrast photo of a <CLS>."	68.53 (+7.81)	37.09 (+4.97)	27.31 (+3.71)
"a blurry photo of a <CLS>."	68.84 (+10.96)	36.80 (+5.33)	26.92 (+3.52)
"a photo of a big <CLS>."	67.49 (+10.10)	35.79 (+4.87)	25.64 (+3.29)

Table 9. Prompt template selection. + denotes the accuracy gain over zero-shot ViT-B/32.

it gets difficult to preserve CLIP’s pre-trained knowledge since the normalization parameters begin to overfit to this

domain. Then, a natural question arises -

*Given that CLIP has been adapted to a specific corruption task, will the zero-shot generalization still hold back on its source test set?*

In this crucial experiment, we challenge our BATCLIP, and evaluate its zero-shot generalization performance back on the source test set, to check the preservation of pre-trained

Dataset	$f_{vis}$ update	$f_{txt}$ update	Ours
CIFAR-10C	✓	✗	72.58
	✓	✓	<b>73.85</b>
CIFAR-100C	✓	✗	41.00
	✓	✓	<b>42.09</b>
ImageNet-C	✓	✗	29.88
	✓	✓	<b>30.72</b>

Table 10. Ablation on  $\mathcal{L}_{pm}$  to demonstrate the need of *bimodal* adaptation of CLIP encoders - using a ViT-B/16 backbone.

CLIP Knowledge. After the adaptation of CLIP on each corruption task, we report the adapted model’s zero-shot performance on its corresponding source test set. We report results for CIFAR-10C and CIFAR-100C in Tables 7 and 8, using ViT-B/16 and ViT-B/32 backbones. For all of the results, we use the prompt template “a photo of a  $\langle \text{CLS} \rangle$ .”. As an example, for CIFAR-10C, upon adaptation of CLIP to *Gaussian noise* following our approach, we report the adapted model’s zero-shot accuracy on its source test set - CIFAR10 test set.

From Table 7, we observe that, on average, there is a 2.91% drop in accuracy compared to a zero-shot evaluation using pre-trained CLIP ViT-B/16. Similarly, for ViT-B/32, we see a drop of about 7.53% in mean accuracy. In Table 8, for CIFAR-100C using a ViT-B/16 backbone, we see an improvement of 0.76% in mean accuracy.

On the whole, we conclude that since the adaptation for a task happens over multiple test batches, the zero-shot performance back on the source data largely depends on the distribution of the image corruption. Overall, ViT-B/16 visual backbones preserve larger amounts of CLIP pre-trained knowledge. This proves the effectiveness of our method BATCLIP, on average.

### 6.3.7. t-SNE visualizations of CIFAR-10C and CIFAR-100C

In this section, we provide illustrations of task-wise t-SNE [49] plots for CIFAR-10C and CIFAR-100C and compare them against zero-shot ViT-B/16. The results are in Figures 11, 12, 13, and 14. Across all corruptions/tasks, BATCLIP learns strong discriminative visual features with a strong image-text alignment and class-level separation. ImageNet-C has 1000 classes, so, we do not provide t-SNE plots to avoid complications. However, the analysis and results carry forward.

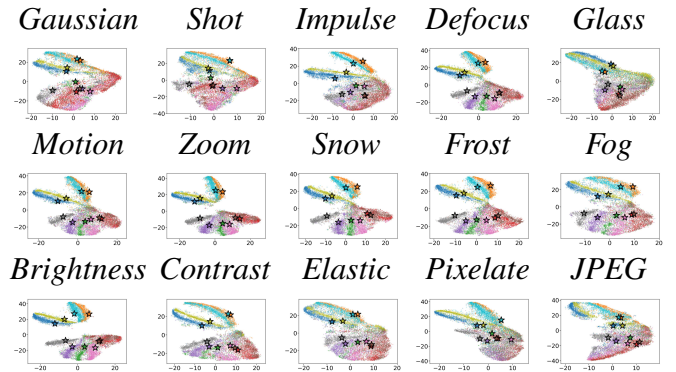


Figure 11. BATCLIP (w/ ViT-B/16): The t-SNE plots show visual ( $\circ$ ) and text ( $\star$ ) features for CIFAR-10C.

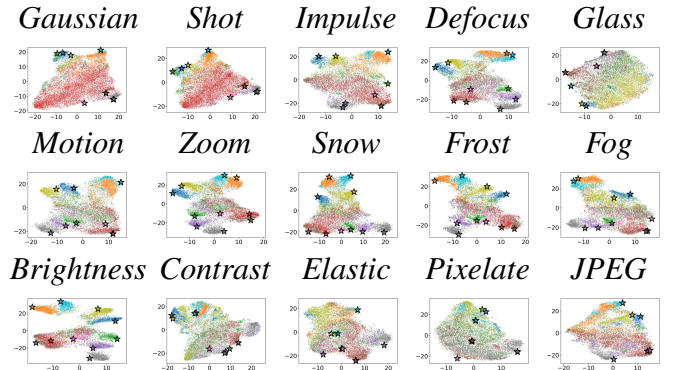


Figure 12. Zero-shot ViT-B/16: The t-SNE plots show visual ( $\circ$ ) and text ( $\star$ ) features for CIFAR-10C.

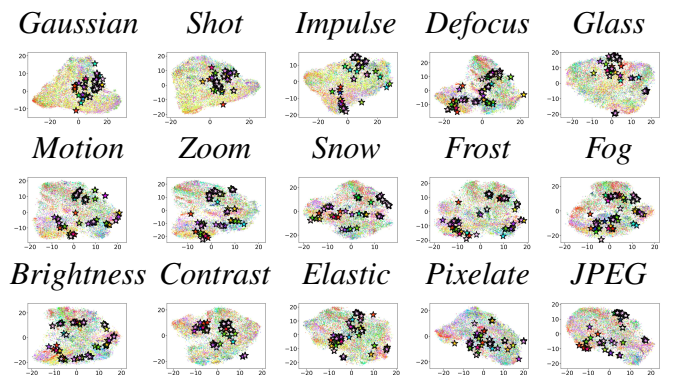


Figure 13. BATCLIP (w/ ViT-B/16): The t-SNE plots show visual ( $\circ$ ) and text ( $\star$ ) features for CIFAR-100C.

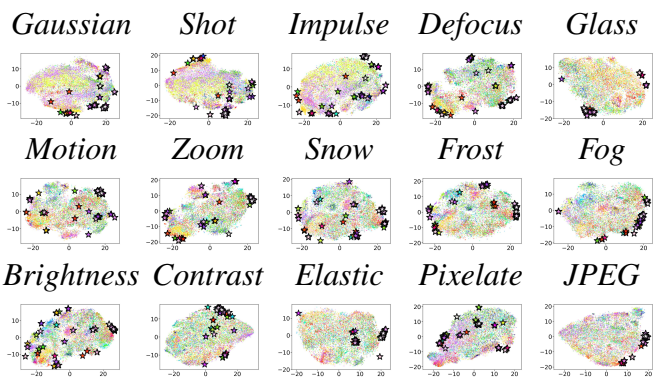


Figure 14. Zero-shot ViT-B/16: The t-SNE plots show visual (○) and text (★) features for CIFAR-100C.